11th Australasian Fluid Mechanics Conference
University of Tasmania, Hobart, Australia
14-18 December 1992

THE ANALYSIS OF PHOTOGRAPHIC DATA OF A VAPOUR CAVITY BUBBLE

S.B. HARVEY[1], J.P. BEST[2] and W.K. SOH[1]

[1]Dept Mechanical Engineering, University of Wollongong, NSW 2521, AUSTRALIA

[2]Maritime Operations Div, MRL/DSTO, Ascot Vale, VIC 3032, AUSTRALIA

ABSTRACT

This paper presents a technique for the analysis of experimental data recording of the surface deformation of a vapour cavity bubble An image analyser is used to digitise the high-speed film frames that record the motion of a bubble near a rigid boundary. Initial results have shown that the digitised images must first be smoothed to reduce the effects of noise. The normal velocity of the bubble surface can be computed from image coordinate data. Along with the coordinate data, this quantity is used as an input to computer code employing a boundary integral method, that solves for the surface velocity potential. Upon substitution of this velocity potential into the Bernoulli equation, the pressure at the surface of the bubble can be found. The fluid is assumed ideal and the flow irrotational.

INTRODUCTION

The deformations and movements of a vapour cavity are important quantities in the understanding of hydraulic cavitation and underwater explosions. Cavitation is known to have a detrimental effect on hydraulic systems such as pumps, spillways and ship propeller blades. Underwater explosion bubbles rapidly displace large volumes of water which have the potential to cause heavy structural damage to marine vessels.

Many computer studies undertaken have furthered understanding of the physics of bubble behaviour. In order to assess the validity of computed results there is a need to reconcile them with experimental data. One area of experimental study is the examination of the evolution of a single bubble near a rigid boundary. The duration of this evolution is about 10 milliseconds. This is far too short for conventional unobstructive pressure and dimensional measurements to be readily made. Instead, high-speed cinematography is used to record the evolution of the bubble.

Benjamin and Ellis (1966) conducted such a study, but Plesset and Chapman (1971) questioned the accuracy of a purely experimental method. Their opinion was that such techniques were difficult and only gave sketchy results. However, it has been found that by combining both experimental (cinematographic) and computational (boundary integral) techniques, the advantages of high-speed photography for this type of work are more fully realised. Indeed, in this study, quantities such as velocity potential, surface pressure and volume have been readily obtained from the digitised images of a vapour cavity.

COMPUTATIONAL TECHNIQUE

As a result of assuming an ideal fluid and irrotational flow, ϕ satisfies Laplace's equation

$$\nabla^2\phi = 0 \qquad (1)$$

It can be shown (Best, 1991a) that the Fredholm integral equation that arises in axisymmetric transient cavity motion problems

$$c(\boldsymbol{p})\phi(\boldsymbol{p}) = \int_S \left(\frac{\partial\phi}{\partial n}(\boldsymbol{q}) G(\boldsymbol{p},\boldsymbol{q}) - \phi(\boldsymbol{q}) \frac{\partial G}{\partial n}(\boldsymbol{p},\boldsymbol{q}) \right) dS(\boldsymbol{q}) \qquad (2)$$

is readily solved for ϕ given $\partial\phi/\partial n$ on S and S, where $\boldsymbol{p}$ is the position vector of a point in the flow domain Ω, and $\boldsymbol{q}$ is the position vector of a point on S. In this work S is the bubble surface and $\partial\phi/\partial n$ the normal surface velocity on S, both of which can be measured from high speed cinematographic data. Let $\boldsymbol{q}'$ be the position vector of the point $\boldsymbol{q}$ reflected about a boundary. Then for the particular case of motion of a vapour cavity near a rigid boundary, the Green's function is defined as

$$G(\boldsymbol{p},\boldsymbol{q}) = \frac{1}{|\boldsymbol{p} - \boldsymbol{q}|} + \frac{1}{|\boldsymbol{p} - \boldsymbol{q}'|} \qquad (3)$$

The function $c(\boldsymbol{p})$ is written as

$$c(\boldsymbol{p}) = 4\pi - \int_S \frac{\partial G}{\partial n}(\boldsymbol{p},\boldsymbol{q}) dS(\boldsymbol{q}) \qquad (4)$$

$$= 4\pi \text{ for } \boldsymbol{p} \text{ in } \Omega \text{ but not on } S$$

$$= 2\pi \text{ for } \boldsymbol{p} \text{ on } S \text{ where } S \text{ is smooth}$$

Code used to solve equation (2) for ϕ given S and $\partial\phi/\partial n$ on S was implemented by Best (1991a) and is used in the present study.

For a sequence of three consecutive images, the notation of the velocity potentials ϕ_{ij} on the initial and final bubble surface nodes are shown in Figure 1. The cylindrical coordinate system is used, and bubble axisymmetry assumed.

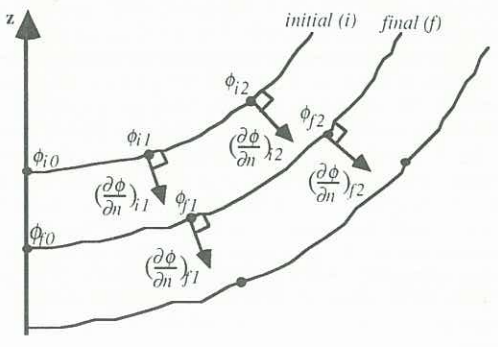

Figure 1. *Nomenclature of bubble surface velocity potentials*

Assuming that the trajectory of a fluid particle at the *initial* (*i*) node *j* is approximately radial to the *final* (*f*) node *j*, the time rate of change of the initial bubble velocity potential can be expressed as

$$\left(\frac{D\phi}{Dt}\right)_{ij} \approx \frac{\phi_{fj} - \phi_{ij}}{\Delta t} \qquad (5)$$

where Δt is the time interval betwen successive photographic images. The approximation given in (5) is adequate for this study because of the spherical shape during the first expansion phase of the bubble. However it is recognised that in order to do the calculation correctly, $\partial\phi/\partial\xi$, the component of the fluid velocity tangential to the bubble surface, would have to be evaluated, where ξ is the arclength parameter. This could then be combined with $\partial\phi/\partial n$ to calculate the trajectory of the *initial* (*i*) node *j*, which would not, in general, be to the *final* (*f*) node *j* as assumed in (5). The actual value of ϕ_{ij} and the new fluid element position would then be found by interpolation, allowing a more accurate value of $(D\phi/Dt)_{ij}$ to be calculated.

The pressure p_{ij} at the nodes of the initial bubble surface can be found by rearranging the Bernoulli equation to

$$p_{ij} = p_\infty - \rho\left(\frac{D\phi}{Dt} - \frac{1}{2}v^2\right)_{ij} - g(z_{ij} - z_0) \qquad (6)$$

where ρ is the fluid density, g is the acceleration due to gravity, z_0 is the free surface vertical coordinate and p_∞ the hydrostatic pressure. We approximate the velocity v by $\partial\phi/\partial n$.

EXPERIMENTAL TECHNIQUE

Whilst vapour cavities have been succesfully grown from small nuclei by the application of negative pressure (Benjamin and Ellis, 1966), a more convenient means of generating a single vapour cavity is by means of the high voltage spark discharge technique as documented by Gibson (1968) and also Wong (1988). Due to the extremely short life of this type of bubble, conventional unobstructive measurements of its geometry and pressure cannot be made without the use of laser techniques. Indeed, pressure transducers in the vicinity of such a bubble have been dislodged due to the sudden release of energy from the spark discharge apparatus.

Perhaps the only other unobstructive means of making the required measurements is by indirectly extracting them from photographic data. The evolution of a typical underwater vapour cavity includes numerous growth and collapse phases. In this study the evolution is recorded at 6000 frames per second, the negatives of the images being post-processed by a digital image analyser on a frame-by-frame basis. Only a two-dimensional study is possible, the bubble surface being assumed axisymmetric.

A certain degree of intelligence is afforded by the analyser in that it is able to distinguish the boundary between the vapour cavity and the surrounding fluid. That is to say, the surface of the bubble is extracted from the film frame negatives and measured relative to some fixed origin.

Nodes are placed upon the bubble surface negative at 10 degree angular intervals in a counterclockwise direction with respect to the centroid. Their cartesian coordinates are measured in pixels from the origin (1 pixel = 0.191571 mm).

Each bubble image is digitised in this way and the cartesian coordinates written to a data file for subsequent computer analysis. During the life of a typical bubble, 165 files are created, each containing 36 nodal coordinates. Due to the orientation of the film frame negatives, the images must undergo a transformation in the vertical plane. A change of axes also takes place so that the new origin resides at the abscissa of the bubble centroid and the ordinate of the rigid boundary.

Smoothing of Data

Due to the presence of experimental noise in the bubble image files, some smoothing of the raw data is necessary before any analysis can be undertaken. The initial smoothing routine consists of a coordinate averaging technique, and is successful to a certain degree in returning the bubble surface to a more spherical form.

A secondary smoothing routine utilising the 5-point formula of Longuet-Higgins and Cokelet (1976), as implemented by Best (1991b), was used to further refine the data. Although both routines removed most of the spurious data, some noise still remained on the bubble surfaces. As discussed later, this noise greatly affected the results from the boundary integral code.

Curve Fitting

Following the mathematical method of Kucera (1992) for representing bubble surfaces, cubic splines are used to fit the nodes of each half-bubble image to a function in ξ, the arclength parameter. Since the bubbles are assumed axisymmetric, only the right-hand half of each smoothed image need be considered. Before the spline-fitting can be carried out, the coordinate system must be transformed from cartesian to cylindrical. The node numbering scheme shown in Figure 2 is employed.

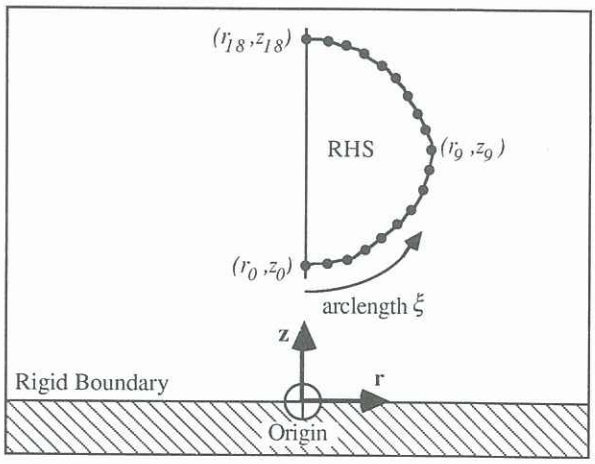

Figure 2. *Axisymmetric node numbering scheme for cubic spline fitting*

The spline functions are expressed as

$$r(\xi) = r_{Aj} + (\xi - \xi_j)(r_{Bj} + (\xi - \xi_j)(r_{Cj} + (\xi - \xi_j)r_{Dj})) \qquad (7)$$

$$z(\xi) = z_{Aj} + (\xi - \xi_j)(z_{Bj} + (\xi - \xi_j)(z_{Cj} + (\xi - \xi_j)z_{Dj})) \qquad (8)$$

for $\xi_j < \xi < \xi_{j+1}$ $\quad j = 0, \ldots, n-1$

where
j = node counter
n = number of nodes = 19
$r_{Aj} \ldots r_{Dj}, z_{Aj} \ldots z_{Dj}$ = spline parameters
ξ_j = arclength of node j

By using equations (7) and (8), interpolation between known node points is possible. The boundary integral code requires the expressing of the bubble surface as a cubic spline.

Calculation of the Bubble Surface Normal Velocity

$\partial\phi/\partial n$ denotes the normal velocity of the bubble surface. It is approximated by first computing the distance d travelled by the surface, and dividing this distance by the timestep Δt. The method used here is a refinement of this simple idea, on a nodal basis, utilising the cubic spline representations of the bubble's surface. In this study, only the first expansion phase of the bubble's life is examined.

If equations (7) and (8) are differentiated with respect to the arclength parameter ξ, the resulting derivatives are given as

$$\frac{dr}{d\xi} = r_{Bj} + 2r_{Cj}(\xi - \xi_j) + 3r_{Dj}(\xi - \xi_j)^2 \quad (9)$$

$$\frac{dz}{d\xi} = z_{Bj} + 2z_{Cj}(\xi - \xi_j) + 3z_{Dj}(\xi - \xi_j)^2 \quad (10)$$

At the node points (r_j , z_j),

$$\frac{dr}{d\xi} = r_{Bj} \quad (11)$$

$$\frac{dz}{d\xi} = z_{Bj} \quad (12)$$

The outward unit normal vector **n** to the bubble's surface at each node point can be written as

$$\mathbf{n}_j = \left(\frac{dz}{d\xi} , \frac{-dr}{d\xi}\right)_j = (z_{Bj} , -r_{Bj}) \quad (13)$$

Consider the sequence of two consecutive expanding bubble surfaces in Figure 3.

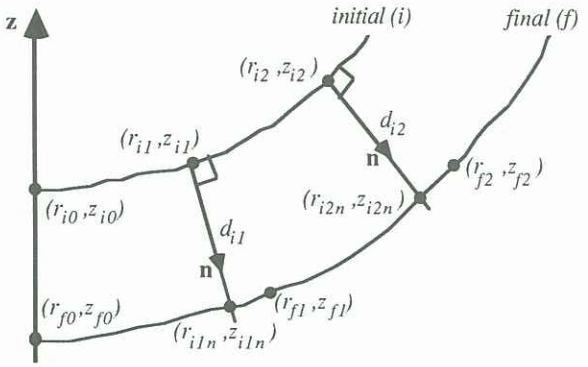

Figure 3. *Calculation of nodal translational distance, normal to the bubble surface*

Let the coordinates of the initial surface of the sequence be (r_{ij} , z_{ij}) and the final surface of the sequence be (r_{fj} , z_{fj}). The point (r_{ijn} , z_{ijn}) represents the intersection of the outward normal from the initial node j with the final bubble surface, which is defined by equations (7) and (8). This intersection point can be found by satisfying the condition

$$\left| \frac{z_{ijn} - z_{ij}}{r_{ijn} - r_{ij}} - \frac{-r_{Bj}}{z_{Bj}} \right| < \varepsilon \quad (14)$$

over $$\xi_j - \tfrac{1}{4}(\xi_j - \xi_{j-1}) < \xi < \xi_j + \tfrac{1}{4}(\xi_{j+1} - \xi_j) \quad (15)$$

for a given small ε. The arc length ξ was found long enough to satisfy equation (14) even for heavily distorted surfaces.

Thus when the slope of the line joining the bubble surfaces from (r_{ij} , z_{ij}) is within ε of being equal to the slope of the outward normal at that node, the intersection point (r_{ijn} , z_{ijn}) has been found. The normal distance d_{ij} is then simply the Euclidian distance between the points (r_{ij} , z_{ij}) and (r_{ijn} , z_{ijn})

$$d_{ij} = \sqrt{(r_{ijn} - r_{ij})^2 + (z_{ijn} - z_{ij})^2} \quad (16)$$

Upon division by the timestep Δt, the normal bubble surface velocity at the node j can be approximated by

$$\left(\frac{\partial \phi}{\partial n}\right)_{ij} \approx \frac{d_{ij}}{\Delta t} \quad (17)$$

RESULTS AND DISCUSSIONS

A validation test was first carried out on the computer code to check its operation, using known analytical solutions. This proved successful and the raw data from the bubble image coordinate files was then read in. Output from the code consisted of volume, normal velocity, velocity potential, time rate of change of velocity potential and surface pressure vs time on a nodal basis.

It is clear from Figure 4 that the bubble undergoes a number of expansion/collapse phases. A similar photographic study by Wong et al. (1989) showed that up to five such pulsations are possible. In this case seven phases were recorded.

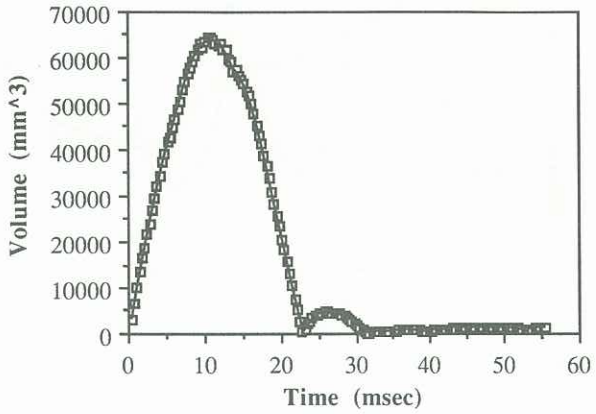

Figure 4. *Bubble volume vs time*

This study is concerned with the first expansion phase only, since after the first collapse the bubble evolves into a toroidal form (Best, 1992), and its internal structure cannot be resolved. To apply the current technique to subsequent phases assumes that the whole outline of the bubble can be seen, which is clearly not the case. The first expansion phase takes place from bubble inception to t = 10.8 msec.

Benjamin and Ellis (1966) noted that the collapse time for a typical vapour cavity was 10 msec. The first collapse phase time of the bubble in the present study is also very close to 10 msec, as seen in Figure 4.

Normal velocity data for the first expansion phase is given in Figure 5. As expected, the normal velocity of the expanding bubble surface is highest immediately after inception. A large drop in normal velocity occurs during the short interval t = 0.5 msec and t = 1.5 msec. An initial normal velocity of around 8 m/s was observed.

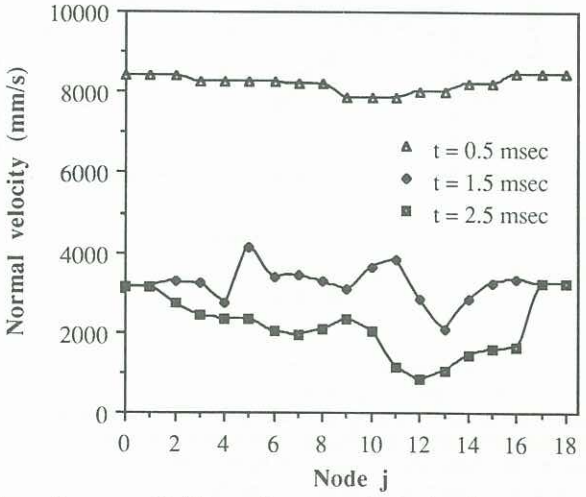

Figure 5. *Bubble surface normal velocity - first expansion phase*

Note that the uniformity in normal velocity measurements has deteriorated rapidly with time. At t = 2.5 msec some noticeable peaks and troughs begin to appear. It is unclear if these are due to poor data quality or if they actually represent velocity fluctuations.

A different trend is observed in the behaviour of the nodal velocity potential in the first expansion phase, as depicted in Figure 6.

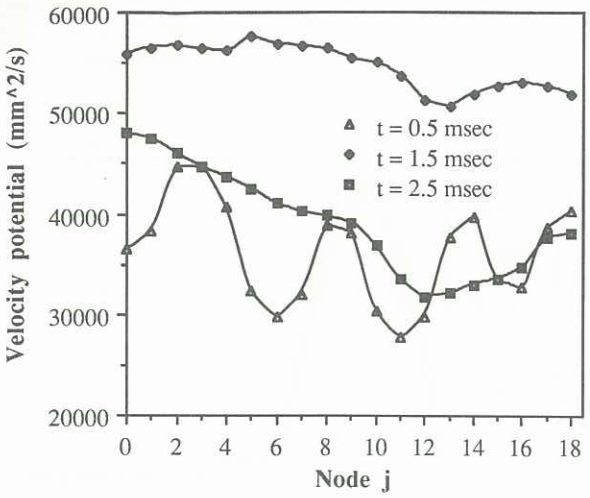

Figure 6. *Computed bubble surface velocity potential - first expansion phase*

A comparison of the curves for t = 0.5 msec and t = 1.5 msec shows that ϕ_{ij} appears to have stabilised with time. Note that the velocity potentials are computed quantities using the boundary integral code.

The surface pressures during the first expansion phase appear to average around 40 kPa, as depicted in Figure 7. The energy loss in the bubble is evident from reductions in volume, normal velocities and nodal pressures.

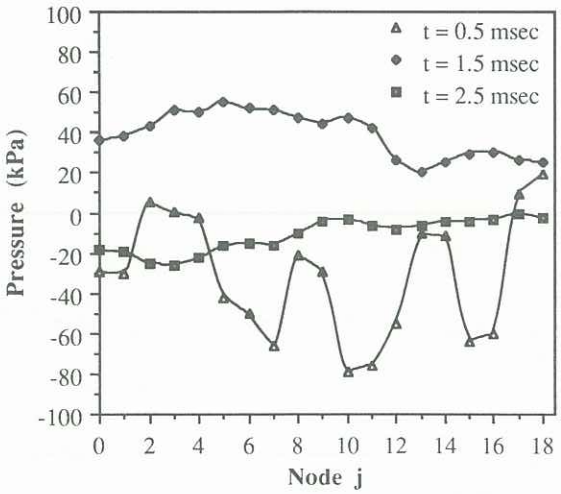

Figure 7. *Computed bubble surface pressure - first expansion phase*

Due to the presence of spurious areas in the photographic data, image analysis was very difficult. This in turn led to poor quality coordinate data, which tended to degrade any numerical results. However this work is only in the preliminary stages and with further improvement of raw data quality more accurate results can be expected.

CONCLUSIONS

By extracting bubble surface coordinate data from high speed film frames, a bubble's volume and normal surface velocity have been found. High speed photography has been shown to be a convenient and unobstructive method for obtaining these quantities. The presence of noise in the photographic data was seen to have a detrimental effect on the computation of nodal velocity potentials and pressures. However, the code appears to smooth the velocity potentials with time. To this end, the boundary integral method has been successfully employed in the analysis of the behaviour of a real vapour cavity near a rigid boundary.

Further work needs to be undertaken in the improvement of photograhic data for image analysis, and the smoothing of any noise in the coordinate files before the boundary integral method is applied. The use of analytically computed data rather than direct experimental data will enable checking of the computational technique without experimental error.

Representation of a bubble's surface may be more readily accomplished by elliptical curve fitting, however this is yet to be proven.

ACKNOWLEDGEMENTS

We wish to acknowledge the contribution of Dr Adam Kucera of the Australian Defence Force Academy in supplying the original boundary integral code for this work, and Mr Darren Wiese of the Materials Research Laboratory who performed the digital image analysis.

REFERENCES

BENJAMIN, T.B. and ELLIS, A.T. (1966) The collapse of cavitation bubbles and the pressures thereby produced against solid boundaries. Phil. Trans. Roy. Soc. A260, 221-240.

BEST, J.P. (1991a) A FORTRAN subroutine for solving a Fredholm intgeral equation of the second kind that arises in axisymmetric free surface flow problems. Technical report, DSTO (MRL), Melbourne.

BEST, J.P. (1991b) The dynamics of underwater explosions. PhD Thesis, University of Wollongong.

BEST, J.P. (1992) The formation of toroidal bubbles upon the collapse of transient cavities. Submitted to J. Fluid Mech.

GIBSON, D.C. (1968) Cavitation adjacent to plane boundaries. Proc. 3rd Aust. Conf. on Hydraulic and Fluid Mechanics, IEAust, Sydney, 210-214.

KUCERA, A. (1992) A boundary integral method applied to the growth and collapse of bubbles near a rigid boundary. Submitted to J. Comp. Phys.

LONGUET-HIGGINS, M.S. and COKELET, E.D. (1976) The deformation of steep surface waves on water. I. A numerical method of computation, Proc. Roy. Soc. A 350, 1-26.

PLESSET, M.S. and CHAPMAN, B. (1971) Collapse of an initially spherical vapour cavity in the neighbourhood of a solid boundary. J. Fluid Mech. 47, 283-290.

WONG, K.C. (1988) High speed flow visualization of a cavitation bubble. B.E. Thesis, University of Wollongong.

WONG, K.C., SOH, W.K., and BLAKE, J.R. (1989) High speed visualization of vapour cavity near boundaries. Proc. 10th Aust. Fluid Mech. Conf., Melbourne, I, 2.27-2.30.